IOPscience iopscience.iop.org

Home Search Collections Journals About Contact us My IOPscience

The short periodic orbit approach for the quantum cat maps

This article has been downloaded from IOPscience. Please scroll down to see the full text article.

2008 J. Phys. A: Math. Theor. 41 405102

(http://iopscience.iop.org/1751-8121/41/40/405102)

View the table of contents for this issue, or go to the journal homepage for more

Download details:
IP Address: 171.66.16.152
The article was downloaded on 03/06/2010 at 07:15

Please note that terms and conditions apply.

IOP PUBLISHING JOURNAL OF PHYSICS A: MATHEMATICAL AND THEORETICAL

J. Phys. A: Math. Theor. **41** (2008) 405102 (24pp) doi:10.1088/1751-8113/41/40/405102

The short periodic orbit approach for the quantum cat maps

Eduardo G Vergini[1,2], David Schneider[2] and Alejandro M F Rivas[2,3]

[1] Departamento de Física, E.T.S.I. Agrónomos, Universidad Politécnica de Madrid, 28040-Madrid, Spain
[2] Departamento de Física, Comisión Nacional de Energía Atómica. Av del Libertador 8250, 1429 Buenos Aires, Argentina
[3] Instituto de Ciencia, Universidad Nacional de General Sarmiento, J M Gutierrez 1150, Argentina

Received 25 June 2008, in final form 13 August 2008
Published 11 September 2008
Online at stacks.iop.org/JPhysA/41/405102

Abstract

The short periodic orbit approach is adapted for the quantum cat maps. The main objective is to explain, in a simple abstract model, the most relevant characteristics of this method which was originally developed for Hamiltonian fluxes. In particular, we describe a semiclassical Hamiltonian formulation to evaluate eigenphases and eigenstates of quantum cat maps. The main advantage of this formulation is that each eigenstate is described in terms of a small number, $N/\ln N$, of short periodic orbits, with N the dimension of the Hilbert space. Moreover, matrix elements can be obtained semiclassically with high accuracy in terms of a very small number, of the order of $\ln^2 N$, of homoclinic and heteroclinic orbits. From the computational point of view, this approach reduces the size of matrices used to the order $N/\ln N$.

PACS numbers: 05.45.Mt, 03.65.Sq

1. Introduction

Gutzwiller's semiclassical trace formula [1] provides the energy spectrum of a classically chaotic Hamiltonian system in terms of the periodic orbits (POs) of the classical system. This formalism was shown to be very efficient for the evaluation of mean properties [2, 3]. Nevertheless, even though it was considerably improved by the use of resummation techniques [4, 5], it suffers from a very serious limitation when a detailed description of properties of the system is required: the number of used POs proliferates exponentially with the Heisenberg time. In this way, the approach loses two common advantages of semiclassical techniques: simplicity in the calculation and more important, simplicity in the interpretation of the results.

Based on numerical experiments in the Bunimovich stadium billiard [6], we have derived a semiclassical theory of short POs [7], which was successfully verified for the first 25

 © 2008 IOP Publishing Ltd Printed in the UK

eigenstates of the stadium [8]. This formalism allows us to obtain all quantum information of a chaotic Hamiltonian system in terms of a very small number of short POs. The essence of the method consists of the construction of wavefunctions related to short unstable POs and the evaluation of matrix elements between these wavefunctions. In 2001, we improved the wavefunction construction by the inclusion of transverse excitations [9] and thereby reducing the energy dispersion by the factor $1/\ln(S/\hbar)$, with S a typical action of the system transverse to the flux, at the considered energy. We have called these optimal wavefunctions *scar functions*, and from now on we will refer to them with the same name.

It is worth emphasizing that a scar function is not only related to a PO, but also to the pieces of stable and unstable manifolds closer to the PO [10]; that is, those pieces of manifolds which can be described in a simple way at semiclassical level. With this picture in mind we were able to analyse the asymptotic behaviour of nondiagonal matrix elements between scar functions [11], observing as a main result that they can be evaluated in terms of a very small number of heteroclinic orbits.

The aim of this paper is to apply the short PO approach to the cat maps in order to show clearly the power of the method. In these maps, the construction of scar functions is trivial, and this fact simplifies the interpretation of the used approximations. On the other hand, as we will employ a semiclassical Hamiltonian formulation for quantizing the map, the obtained results are not exact, as it is for the standard semiclassical quantizations of cat maps. However, this fact is not an obstacle, because the computed errors are much smaller than the typical error found in semiclassical calculations of chaotic systems.

The paper is organized as follows. Section 2 is devoted to describe the used quantized cat map and its associated classical hyperbolic Hamiltonian in the plane. Section 3 explains the scar function construction for our quadratic hyperbolic Hamiltonian in the plane. In section 4, we construct scar functions of POs on the torus and discuss its improvement by using time reversal and spatial symmetry. In section 5, we develop a semiclassical Hamiltonian formulation of the cat map and rewrite matrix elements between scar functions in a convenient way for asymptotic approximations. Section 6 develops the semiclassical evaluation of matrix elements as an asymptotic expansion in powers of $\hbar$. Section 7 is devoted to verify in simple cases, the obtained semiclassical expressions. In section 8, we compare the Hamiltonian calculation of eigenvectors and eigenphases with the exact results. Section 9 is devoted to final remarks and conclusions. We also include six appendices in order to clarify the derivation of the used expressions.

2. The cat maps

The cat maps are the hyperbolic automorphisms of the unit 2-torus. They are completely chaotic dynamical systems for which the torus is the phase space. A quantization procedure for these maps was developed in [12], and we will employ the simplest cat map quantizable by this procedure. It is characterized by the following quantum propagator in the position representation:

$$U_{q',q} = (-\mathrm{i}/N)^{1/2} \exp[\mathrm{i}2\pi N(q^2 - qq' + q'^2)],$$

with $q, q' = 0, 1/N, 2/N, \ldots, (N-1)/N$. The integer N represents the dimension of Hilbert space, and is related to Planck's constant by $\hbar = 1/(2\pi N)$.[4] Furthermore, the wavefunctions are periodic with period 1, and can be non-zero only at rational positions with denominator N.

[4] In general, we will use $\hbar$ for expressions in the plane and N for expressions on the torus.

Let $\{\phi_\mu\}$ be the set of eigenfunctions of the propagator, with $\{\alpha_\mu\}$ the corresponding set of eigenphases satisfying

$$\sum_{k=0}^{N-1} U_{\frac{j}{N},\frac{k}{N}}\phi_\mu(k/N) = \mathrm{e}^{\mathrm{i}\alpha_\mu}\phi_\mu(j/N), \qquad \text{for} \quad j = 0, 1, \ldots, N-1. \tag{1}$$

This set can be decomposed into two symmetry classes according to the following relations: $\phi_\mu(j/N) = \phi_\mu(1 - j/N)$ for even eigenfunctions, and $\phi_\mu(j/N) = -\phi_\mu(1 - j/N)$ for odd ones.

Our objective is to find this set of eigenfunctions and the corresponding eigenphases by using the short PO approach. Now, in order to think about eigenenergies, E_μ, we compare the relation $\hat{U}^t = \exp(-\mathrm{i}\hat{H}t/\hbar)$ (valid for autonomous Hamiltonian systems) with equation (1) to provide the following definition:

$$E_\mu \equiv -\frac{\alpha_\mu \hbar}{\tau}, \tag{2}$$

where τ is the time between consecutive steps of the map. Of course, we have the problem that the spectrum of eigenenergies is periodic. However, such a problematic situation should disappear if we use an energy window much smaller than $2\pi\hbar/\tau$ for the quantum mechanical computation.

The classical mechanics of the system is given by the map that evolves the point (q, p) on the torus ($0 \leqslant q, p < 1$) towards the point (q', p') satisfying the following relations:

$$q' = 2q + p - m \qquad \text{and} \qquad p' = 3q + 2p - n, \tag{3}$$

with the integers m and n imposing the conditions $0 \leqslant q', p' < 1$. The corresponding action is given by

$$R(q', q, m, n) = q^2 - q(q' + m) + (q' + m)^2 - nq', \tag{4}$$

from which the map may be obtained using $p = -\partial R/\partial q$ and $p' = \partial R/\partial q'$. Moreover, if we allocate an energy E to the motion, the reduced action results

$$S(q', q, m, n) = \tau E + R(q', q, m, n). \tag{5}$$

This map corresponds to viewing stroboscopically at time intervals τ, the motion generated by the quadratic Hamiltonian

$$H(q, p) = \frac{\lambda}{2}\left[\left(\frac{p}{\alpha}\right)^2 - (\alpha q)^2\right], \tag{6}$$

with both q and p taken modulo 1 at each observation. $\lambda = \ln(2 + \sqrt{3})/\tau$ is the Lyapunov exponent of the map, and $\alpha = 3^{1/4}$. This Hamiltonian describes, in the plane (q, p), a hyperbolic point at the origin with stable and unstable manifolds given by the straight lines, $p = -\alpha^2 q$ and $p = \alpha^2 q$, respectively. These manifolds are characterized by the stable and unstable vectors,

$$\xi_s = \frac{1}{\sqrt{2}}\left(-\frac{1}{\alpha}, \alpha\right) \qquad \text{and} \qquad \xi_u = \frac{1}{\sqrt{2}}\left(\frac{1}{\alpha}, \alpha\right),$$

normalized by the relation $\xi_u \wedge \xi_s = 1$. These vectors evolve in the plane without modifying their directions, according to the simple rule

$$\xi_s(t) = \mathrm{e}^{-\lambda t}\xi_s \qquad \text{and} \qquad \xi_u(t) = \mathrm{e}^{\lambda t}\xi_u. \tag{7}$$

We note that the previous relations are written by fixing the units of length and momentum to the dimensions of the 2-torus. On the other hand, we do not fix the unit of time in order to clearly show the derivation of a Hamiltonian formulation. Of course, the natural unit of time is τ; by using this, we should replace τ by 1 in all the expressions.

3. The scar function of a hyperbolic point in the plane

In this section, we construct the scar function of the hyperbolic point specified by the classical Hamiltonian of equation (6), with the quantum Hamiltonian,

$$\hat{H} = \frac{\lambda}{2}\left[-\frac{\hbar^2}{\alpha^2}\frac{\mathrm{d}^2}{\mathrm{d}q^2} - (\alpha q)^2\right].$$

Let $\varphi(q,t)$ be the following wave packet:

$$\varphi(q,t) = \frac{1}{(\pi\hbar)^{1/4}\sqrt{\mathrm{e}^{\mathrm{i}\pi/4}Q(t)}}\exp\left[\mathrm{i}\frac{q^2}{2\hbar}\frac{P(t)}{Q(t)}\right] \tag{8}$$

depending on the parameter t, where the complex numbers $Q(t)$ and $P(t)$ are the position and momentum components of the complex vector:

$$(Q(t), P(t)) \equiv \xi_u(t) + \mathrm{i}\xi_s(t).$$

A straightforward calculation shows that $\varphi(q,t)$ verifies the time-dependent Schrödinger equation.

By replacing (7) in (8), one obtains

$$\varphi(q,t) = \frac{\sqrt{\alpha}\,\mathrm{e}^{-\frac{\mathrm{i}}{2}\arctan[\tanh(\lambda t)]}}{[\pi\hbar\cosh(2\lambda t)]^{1/4}}\exp\left\{\left[-\frac{1}{\cosh(2\lambda t)} + \mathrm{i}\tanh(2\lambda t)\right]\frac{(\alpha q)^2}{2\hbar}\right\},$$

where we have selected the phase of $\sqrt{\mathrm{e}^{\mathrm{i}\pi/4}Q(t)}$ in the range $(-\pi/8, \pi/8)$ in order to obtain a continuous function of t. From this relation, we inmediately note that the dispersion in q increases exponentially with t:

$$\sigma_q(t) = \sqrt{\frac{\hbar\cosh(2\lambda t)}{2\alpha^2}}. \tag{9}$$

Moreover, the following relations can be verified[5]:

$$\int_{-\infty}^{\infty}\varphi^*(q,t)\varphi(q,t)\,\mathrm{d}q = 1,$$

$$\int_{-\infty}^{\infty}\varphi^*(q,t)\hat{H}\varphi(q,t)\,\mathrm{d}q = 0,$$

$$\int_{-\infty}^{\infty}\varphi^*(q,t)\hat{H}^2\varphi(q,t)\,\mathrm{d}q = (\hbar\lambda)^2/2,$$

and with them the energy dispersion of $\varphi(q,t)$ results

$$\sigma_E = \frac{\lambda\hbar}{\sqrt{2}}. \tag{10}$$

We emphasize that this is a minimum value; that is, the energy dispersion of an arbitrary wave packet is strictly greater than the previous value.

Then, with this optimal wave packet at hand, we define the scar function by the following integral representation:

$$\phi(q) \equiv K\int_{-T}^{T}\cos\left(\frac{\pi t}{2T}\right)\varphi(q,t)\,\mathrm{d}t, \tag{11}$$

with K the positive real number that normalizes $\phi(q)$ to unity. As the imaginary part of $\varphi(q,t)$ is an odd function of t, $\phi(q)$ is real function of q. Moreover, as $\varphi(q,t)$ is even with respect to

[5] As $\varphi(q,t) = \exp[-(\mathrm{i}/\hbar)\hat{H}t]\varphi(q,0)$, it is sufficient to verify these relations for $t = 0$.

$q, \phi(q)$ is also even; note that this property is independent of the used quadratic Hamiltonian. Finally, the action of $\hat{H}$ on $\phi(q)$ defines the wavefunction:

$$h(q) \equiv \hat{H}\phi(q). \tag{12}$$

We have proved in [11] that $\phi(q)$ is the wavefunction with minimum energy dispersion among all the constructions that use $\varphi(q, t)$ for times $|t| \leqslant T$.[6] This result is asymptotically valid, and the leading order of the energy dispersion, as $T \to \infty$, is given by

$$\sigma_E(T) = \left[\int_{-\infty}^{\infty} \phi^*(q)\hat{H}^2\phi(q)\,\mathrm{d}q\right]^{1/2} \simeq \frac{\pi\hbar}{2T}. \tag{13}$$

In appendix A, we develop an interpolation formula connecting the limiting cases $T \to 0$ and $T \to \infty$ given by equations (10) and (13), respectively.

In order to estimate the area A over which the scar state is extended in phase space, we use the following relation:

$$T = \frac{\ln(A/\hbar)}{2\lambda}. \tag{14}$$

For $T = 0$, the wave packet does not evolve, thus the state occupies an area equal to $\hbar$. For $A = 1$, the wave packet is able to evolve up to the border of the square representing the 2-torus for the map, and the corresponding time is the so-called Ehrenfest time T_E. Of course, it is simple to evaluate the scar state for areas greater than 1, because the manifolds are straight lines and we will do that in the numerical calculations. However, the manifolds of generic chaotic systems are very complex objects, and then, the evaluation of scar states for times greater than T_E is extremely difficult; by the way, we will show that this operation is not very useful.

We mention that our original scar function construction (see [9] or [11]) is a linear combination of some eigenfunctions of the harmonic oscillator $(\lambda/2)(p^2/\alpha^2 + \alpha^2 q^2)$; those eigenfunctions living inside an area A of the plane q–p around the origin. Moreover, the coefficients of the combination are obtained by minimizing the energy dispersion. Even though the original scar function has an energy dispersion smaller than $\phi(q)$ for finite values of $\hbar$, they have the same asymptotic behaviour given by equation (13); in [11], we provide an extensive comparison of these two constructions. So, to simplify the mathematical content of this paper, we use equation (11) as our definition of scar function of the considered hyperbolic point. Nevertheless, it should be clear that it is possible to use our original definition in the following section.

4. The scar function of periodic orbits on the torus

A wavefunction defined in the plane is projected on the torus by periodizing the function in q and p. For this reason our starting point is the scar function $\phi(q)$ defined in the previous section.

Let γ be a primitive PO of the map with n different points on the torus:

$$(q_0, p_0), (q_1, p_1), \ldots, (q_{n-1}, p_{n-1}), (q_n = q_0, p_n = p_0).$$

Then, a scar function of γ is defined by the following simple expression (the meaning of this expression is discussed in the following section):

$$\phi_\gamma(q) \equiv \frac{1}{\sqrt{n}} \sum_{j=0}^{n-1} \mathrm{e}^{\mathrm{i}S_j/\hbar}\, \mathrm{e}^{\mathrm{i}p_j(q-q_j)/\hbar}\phi(q - q_j), \tag{15}$$

[6] The parameter T used in equation (11) is $1/2\lambda$ times the parameter T used in [11].

where S_j is the reduced action for going from q_0 to q_j. That is $S_0 = 0$, and from equation (5) one obtains

$$S_j = j\tau E_\gamma + \sum_{k=0}^{j-1} R(q_{k+1}, q_k, m_k, n_k), \qquad \text{for} \quad j \geqslant 1, \tag{16}$$

where E_γ is the so-called Bohr–Sommerfeld (BS) energy of γ. There are n different BS energies related to γ, and they are obtained from the BS quantization rule:[7]

$$S_n/\hbar = 2\pi m, \qquad \text{with} \quad m \quad \text{integer}. \tag{17}$$

By replacing equation (16) in (17) it is possible to write E_γ, or just the corresponding BS phase α_γ,[8] explicitly as follows:

$$\alpha_{\gamma,m} \equiv -\frac{\tau E_{\gamma,m}}{\hbar} = -\frac{2\pi m}{n} + \frac{1}{n\hbar}\sum_{k=0}^{n-1} R(q_{k+1}, q_k, m_k, n_k) \pmod{2\pi}, \tag{18}$$

for $m = 0, 1, \ldots, n-1$.

The projection of $\phi_\gamma(q)$ on the torus is obtained by making the function periodic in p, which consists in taking rational positions with denominator N, and also in q by summing on integer translations. This yields

$$\overline{\phi}_\gamma(k/N) \equiv \sum_{l=-\infty}^{\infty} \phi_\gamma(k/N - l), \qquad \text{for} \quad k = 0, 1, \ldots, N-1, \tag{19}$$

where the sum can be reduced to three terms ($l = -1, 0$ and 1) for times $T < T_E$. However, in the general case, it is necessary to include all the terms satisfying $|l| \lesssim 1 + \mathrm{e}^{\lambda(T-T_E)}$.[9] This means that even though scar functions of cat maps are described by very simple expressions, the computation for times greater than the Ehrenfest time results involved (the number of relevant terms in (19) increases exponentially with T).

It is possible to improve the scar function construction by using time reversal and spatial symmetry. Time reversal leads to real scar functions, and spatial symmetry projects them into one of the two symmetry classes mentioned in section 2. The used recipes, exactly equivalent to those applied to Hamiltonian fluxes, are briefly described below; a deeper account is provided in appendix F.

Let γ^* and γ' be the POs connected to γ by spatial symmetry and time reversal, respectively; that is, γ^* contains the points $(q_j^* = 1 - q_j, p_j^* = 1 - p_j) \pmod 1$, and γ' the points $(q_j' = q_{j'}, p_j' = 1 - p_{j'}) \pmod 1$, with $j' = n - j \pmod n$. If γ has no symmetries at all, it is necessary to use a linear combination of four scar functions related to the set of POs $\{\gamma, \gamma^*, \gamma', \gamma^{*\prime}\}$ in order to obtain real functions within defined symmetry classes; however, this case is only required at extremely large values of N ($\gtrsim 10^4$ for the cat map considered in this paper). On the other hand, if γ is time reversal invariant ($\gamma = \gamma'$), a linear combination of the scar functions related to the set $\{\gamma, \gamma^*\}$ (which are real functions up to a global phase) provides the required symmetry class; section 8 shows an example. Equivalently, if $\gamma = \gamma^{*\prime}$, scar functions corresponding to the set $\{\gamma, \gamma^*\}$ are, after adding a global phase, complex conjugated with the real part being even and the imaginary part being odd (in section 8 we provide an example)[10]. Finally, when the PO simultaneously satisfies time reversal and spatial

[7] The Bohr–Sommerfeld rule selects those energies for which the accumulated phase along the periodic orbit is a multiple of 2π.

[8] α_γ is defined in accordance with equation (2).

[9] This relation is derived from (9) and the definition of T_E is given in (14).

[10] For the cat map used in this paper, the $\gamma = \gamma^* \neq \gamma'$ case, which is not explicitly considered, only occurs for $n \geqslant 8$; see appendix F.

symmetry, the associated scar function is a real (up to a global phase) function, even or odd depending on the BS phase; see section 7.

We finish this section by noting that the meaning of the length of a PO, when symmetries are present, is different in our approach from that used by Gutzwiller. In Gutzwiller's theory, the length of a PO is related to its stability $e^{\lambda\tau n}$, and so is directly given by n. In our approach, the length of a PO is related to the complexity of the corresponding scar function and so, we have to sum the periods of all the POs used in the construction. For instance, if γ has no symmetries, the corresponding length is $4n$ according to our viewpoint.

5. A Hamiltonian formulation for the cat maps

The main idea behind the construction of wavefunctions of unstable POs is the decomposition of the motion in the vicinity of the central PO into one of periodic nature and other of hyperbolic character. In [7], we obtained explicitly such decomposition for two degrees of freedom autonomous Hamiltonian systems. Furthermore, such decomposition can be extended to more degrees of freedom in an almost straightforward way; this is the content of Floquet's theorem [13].

The motion of periodic nature is related to the topological structure of the orbits in the vicinity of the central PO; in other words, it provides the evolution of the stable and unstable directions as we move along the PO. In particular, such directions are fixed for the cat maps, and then the evolution of orbits in the vicinity of the PO is simply described by the motion of hyperbolic character.

In order to develop these ideas, let us assume that the classical structure of the cat maps is derived from a Hamiltonian flux, with the 2-torus being a particular Poincaré surface of section. Then, let us describe the motion in the vicinity of γ in terms of local coordinates. The variable x parameterizes γ, for instance, x can be the time that now is continuous, and p_x is the corresponding momentum. The variables in the transverse direction to γ are given by y and p_y; we assume that $y = 0$ on γ, and so $\dot{y}$ is also zero on γ. Then, the motion in the neighbourhood of γ is described by the following local Hamiltonian[11]:

$$H_\gamma(x, p_x, y, p_y) = H_{||}(x, p_x) + H(y, p_y),$$

with H the hyperbolic Hamiltonian of equation (6); so, $p_y = \alpha^2\dot{y}/\lambda$ is equal to zero on γ. $H_{||}(x, p_x)$ is an unknown one-dimensional Hamiltonian along γ, from which we only know the corresponding action between points on the Poincaré surface of section. Note that in the neighbourhood of (q_j, p_j), the local variables are

$$x = j\tau, \qquad y = q - q_j \qquad \text{and} \qquad p_y = p - p_j.$$

Let us define a closed path in the neighbourhood of γ by a translation of γ in the transverse direction; this means to change the transverse variables from zero to given values y and p_y, these values being the label for the path. A closed path is invariant by the action of $H_{||}(x, p_x)$, while it evolves into another closed path by the action of $H(y, p_y)$; the evolution is dictated by the evolution of the label (y, p_y). Then, the intersection of a closed path with the surface of section consists of n points with coordinates $(q = y + q_j, p = p_y + p_j)$ (mod 1) for $j = 0, \ldots, n-1$, and these intersecting points evolve continuously on the torus under the action of $H(y, p_y)$.

In this way, we have established a Hamiltonian formulation on the torus; of course, it only works for closed paths. Nevertheless, as the scar function construction of equation (15) is supported by a bunch of closed paths, we can also employ this Hamiltonian formulation at

[11] See equation (15) of [9] for an explicit expression of H_γ in the case of Hamiltonian fluxes.

quantum level. In order to clarify this point, we note that a scar function consists of the local plane–wave approximation, $e^{iS(x)/\hbar}$,[12] along the bunch of closed paths with energy E_γ, and the translation of $\phi(q)$ to each point on γ in the transverse direction. Specifically, the scar function in local coordinates is given by[13]

$$\phi_\gamma(x, y) = \frac{1}{\sqrt{n}} e^{iS(x)/\hbar}\phi(y),$$

and with this, the action of $\hat{H}_\gamma$ is simply taken into account by $\hat{H}_{||}\, e^{iS(x)/\hbar} = E_\gamma\, e^{iS(x)/\hbar}$ and $\hat{H}\phi(y) = h(y)$, with $h(y)$ defined in equation (12). This yields

$$\hat{H}_\gamma\phi_\gamma(x, y) = E_\gamma\phi_\gamma(x, y) + \frac{1}{\sqrt{n}} e^{iS(x)/\hbar}h(y),$$

which in terms of the global coordinate q on the surface of section results

$$\hat{H}_\gamma\phi_\gamma(q) = E_\gamma\phi_\gamma(q) + h_\gamma(q), \tag{20}$$

with

$$h_\gamma(q) = \frac{1}{\sqrt{n}} \sum_{j=0}^{n-1} e^{iS_j/\hbar}\, e^{ip_j(q-q_j)/\hbar}h(q - q_j).$$

The wavefunction obtained in equation (20) is defined in the real line. So, by periodizing this function in p and q, we get a Hamiltonian formulation for the quantum cat maps[14]:

$$\hat{H}_{\rm cat}\overline{\phi}_\gamma(k/N) \equiv E_\gamma\overline{\phi}_\gamma(k/N) + \overline{h}_\gamma(k/N), \qquad \text{for} \quad k = 0, 1, \ldots, N-1. \tag{21}$$

This equation contains one of the main ideas behind the short PO approach; the action of the Hamiltonian of the system, $\hat{H}_{\rm cat}$, acting on a scar function of γ is taken into account through its local version.

Matrix elements between scar states are given by

$$\langle\delta|\gamma\rangle = \frac{1}{N}\sum_{k=0}^{N-1}\overline{\phi}^*_\delta(k/N)\overline{\phi}_\gamma(k/N), \tag{22}$$

$$\langle\delta|\hat{H}_{\rm cat}|\gamma\rangle = \frac{1}{N}\sum_{k=0}^{N-1}\frac{1}{2}[\overline{\phi}^*_\delta(k/N)\hat{H}_{\rm cat}\overline{\phi}_\gamma(k/N) + \hat{H}_{\rm cat}\overline{\phi}^*_\delta(k/N)\overline{\phi}_\gamma(k/N)], \tag{23}$$

$$\langle\delta|\hat{H}^2_{\rm cat}|\gamma\rangle = \frac{1}{N}\sum_{k=0}^{N-1}\hat{H}_{\rm cat}\overline{\phi}^*_\delta(k/N)\hat{H}_{\rm cat}\overline{\phi}_\gamma(k/N), \tag{24}$$

with δ a primitive periodic orbit of the map[15]. In equation (23), we have symmetrized the Hamiltonian matrix element to guarantee Hermiticity.

The previous expressions can be written in a convenient way in order to apply asymptotic expansions. By using equations (B.1), (B.2) and (21), we rewrite them as follows:

$$\langle\delta|\gamma\rangle = \sum_{j,l=-\infty}^{\infty}\int_{-\infty}^{\infty}\phi^*_\delta(q)\, e^{ijq/\hbar}\phi_\gamma(q - l)\, dq, \tag{25}$$

[12] Actually, the local plane–wave approximation is given by $e^{iS(x)/\hbar}/\sqrt{\dot{x}}$, so we are assuming that $\dot{x}$ is constant along γ.

[13] A deeper explanation of this construction and the meaning of closed path can be found in the appendix B of [11].

[14] Even though the notation is clear, we remark that $\overline{h}_\gamma(k/N) = \sum_{l=-\infty}^{\infty} h_\gamma(k/N - l)$.

[15] The inclusion of the factor $1/N$ in the definition of matrix elements guarantees the normalization of the scar functions in leading order; that is, $\langle\gamma|\gamma\rangle \to 1$ for $N \to \infty$.

$$\langle\delta|\hat{H}_{\rm cat}-(E_\delta+E_\gamma)/2|\gamma\rangle=\sum_{j,l=-\infty}^{\infty}\int_{-\infty}^{\infty}\mathrm{e}^{\mathrm{i}jq/\hbar}[\phi_\delta^*(q)h_\gamma(q-l)+h_\delta^*(q)\phi_\gamma(q-l)]\frac{\mathrm{d}q}{2}, \quad (26)$$

$$\langle\delta|(\hat{H}_{\rm cat}-E_\delta)(\hat{H}_{\rm cat}-E_\gamma)|\gamma\rangle=\sum_{j,l=-\infty}^{\infty}\int_{-\infty}^{\infty}h_\delta^*(q)\mathrm{e}^{\mathrm{i}jq/\hbar}h_\gamma(q-l)\,\mathrm{d}q, \quad (27)$$

where the relevant terms are those satisfying $|j|/\sqrt{3}$, $|l|\lesssim 1+\mathrm{e}^{\lambda(T-T_E)}$.[16]

After replacing in equation (25) the expressions given for ϕ_γ and ϕ_δ, in accordance with (15), the overlap results

$$\langle\delta|\gamma\rangle=\frac{1}{\sqrt{n_\delta n_\gamma}}\sum_{j,l}\sum_{m=0}^{n_\delta-1}\sum_{m'=0}^{n_\gamma-1}\mathrm{e}^{\mathrm{i}(S_{m'}-S_m)/\hbar}\times\int_{-\infty}^{\infty}\mathrm{e}^{-\mathrm{i}p_m(q-q_m)/\hbar}\phi^*(q-q_m)\,\mathrm{e}^{\mathrm{i}jq/\hbar}\,\mathrm{e}^{\mathrm{i}p_{m'}(q-l-q_{m'})/\hbar}\phi(q-l-q_{m'})\,\mathrm{d}q.$$

Moreover, rearranging factors and renaming $q-q_m$ with q, one obtains

$$\langle\delta|\gamma\rangle=\frac{1}{\sqrt{n_\delta n_\gamma}}\sum_{j,l}\sum_{m=0}^{n_\delta-1}\sum_{m'=0}^{n_\gamma-1}\mathrm{e}^{\mathrm{i}(S_{m'}+jq_{m'}-S_m-p_mq_0-p_0q_0/2)/\hbar}I_0, \quad (28)$$

where

$$I_0=\int_{-\infty}^{\infty}\phi^*(q)\,\mathrm{e}^{\mathrm{i}p_0(q-q_0/2)/\hbar}\phi(q-q_0)\,\mathrm{d}q, \quad (29)$$

with

$$q_0=q_{m'}+l-q_m \qquad \text{and} \qquad p_0=p_{m'}+j-p_m. \quad (30)$$

The integral I_0 is real because its integrand at $q=q_0/2+\delta q$ is the complex conjugate of the integrand at $q=q_0/2-\delta q$ (remember that ϕ is even). In fact, we have extracted the phase $(S_{m'}+jq_{m'}-S_m-p_mq_0-p_0q_0/2)/\hbar$ of the integral in order to satisfy such a condition. The meaning of this phase is discussed in [11] (in particular, see equation (A.6) in [11]).

In the same way, matrix elements provided by equations (26) and (27) can be obtained from the right-hand side of equation (28) by replacing I_0 with I_1 and I_2, respectively, where

$$I_1=\int_{-\infty}^{\infty}\mathrm{e}^{\mathrm{i}p_0(q-q_0/2)/\hbar}[\phi^*(q)h(q-q_0)+h^*(q)\phi(q-q_0)]\frac{\mathrm{d}q}{2},$$

and

$$I_2=\int_{-\infty}^{\infty}h^*(q)\,\mathrm{e}^{\mathrm{i}p_0(q-q_0/2)/\hbar}h(q-q_0)\,\mathrm{d}q.$$

By using the same argument applied to I_0, it is easy to verify that these integrals are real numbers.

6. Semiclassical evaluation of matrix elements

In this section, we evaluate the integrals I_0, I_1 and I_2 defined in the last section, as an expansion in powers of $\hbar$. To do so, we first apply the symplectic transformation,

$$u=\tfrac{1}{\sqrt{2}}(\alpha q+p/\alpha) \qquad s=\tfrac{1}{\sqrt{2}}(-\alpha q+p/\alpha), \quad (31)$$

[16] These estimates are derived from the dispersion in p and q, for the wave packet $\varphi(q,t=T)$.

with $\alpha = 3^{1/4}$, where u and s are variables leaving along the manifold directions ξ_u and ξ_s, respectively. The reason for this transformation is that $\phi(q)$ is a rapidly oscillating function while the u-representation of the scar state, $\phi_u(u)$, is a slowly varying function far from the origin (see figure 2 of [11]). In order to have some intuition, we mention that an elementary semiclassical estimate of these functions gives us $\phi(q) \sim \cos(\alpha^2 q^2/2\hbar - \pi/4)/\sqrt{|q|}$ and $\phi_u(u) \sim 1/\sqrt{|u|}$, for $|q|, |u| > 2\pi\hbar$.

The Hamiltonian of equation (6) is transformed into λus and the corresponding scar function, $\phi_u(u)$, was extensively studied in [11]. Specifically, we can write (see equation (38)[17] of [11])

$$\phi_u(u) = K \int_{-T}^{T} \cos\left(\frac{\pi t}{2T}\right) \varphi_u(u, t)\, \mathrm{d}t, \tag{32}$$

with

$$\varphi_u(u, t) = \frac{1}{(\pi\hbar)^{1/4}} \exp\left[-\frac{u^2\, \mathrm{e}^{-2\lambda t}}{2\hbar} - \frac{\lambda t}{2}\right],$$

and K the same factor of equation (11). Moreover, the action of the quantum Hamiltonian, $-\mathrm{i}\lambda\hbar(1/2 + u\, \mathrm{d}/\mathrm{d}u)$, on $\phi_u(u)$ directly gives us the u-representation of $h(q)$:

$$h_u(u) = -\mathrm{i}\lambda\hbar \left[\phi_u(u)/2 + u\phi_u^{(1)}(u)\right]. \tag{33}$$

In terms of $\phi_u(u)$, the integral of equation (29) takes the form[18]

$$I_0 = \int_{-\infty}^{\infty} \phi_u^*(u)\, \mathrm{e}^{\mathrm{i}s_0(u-u_0/2)/\hbar} \phi_u(u - u_0)\, \mathrm{d}u, \tag{34}$$

where (u_0, s_0) is obtained from (q_0, p_0) (see (30)) through the transformation (31). To prove the validity of equation (34), it is necessary to verify the following relation between overlaps of wave packets:

$$\int_{-\infty}^{\infty} \varphi_u^*(u, t)\, \mathrm{e}^{\mathrm{i}s_0(u-u_0/2)/\hbar} \varphi_u(u - u_0, t')\, \mathrm{d}u = \int_{-\infty}^{\infty} \varphi^*(q, t)\, \mathrm{e}^{\mathrm{i}p_0(q-q_0/2)/\hbar} \varphi(q - q_0, t')\, \mathrm{d}q$$

for arbitrary times, t and t'. Actually, it is sufficient to verify the previous relation for $t = t' = 0$, because $\varphi(q, t)$ and $\varphi_u(u, t)$ satisfy the corresponding time dependent Schrödinger equations.

In order to understand the semiclassical evaluation of equation (34), let us describe figure 1, where full lines indicate pieces of unstable manifolds, and dashed lines correspond to pieces of stable ones. The cross at the origin is related to the scar function $\phi_u(u)$, and the other cross at (u_0, s_0) represents the scar function,

$$\phi'_u(u) \equiv \mathrm{e}^{\mathrm{i}s_0(u-u_0/2)/\hbar} \phi_u(u - u_0); \tag{35}$$

in this way, I_0 is the overlap $\langle\phi|\phi'\rangle$. Furthermore, there are two intersections between the crosses, one at the heteroclinic point $(u_0, 0)$ and the other at the heteroclinic point $(0, s_0)$; as we will see below, the main contribution to the overlap is concentrated in the neighbourhood of each of these points.

By appropriate transformations of equation (34), it is possible to capture with high accuracy the contribution to I_0 of each heteroclinic point by the method of stationary phase. For instance, as the point $(0, s_0)$ is the intersection of the stable manifold starting at the origin with the unstable manifold starting at (u_0, s_0), we can write $I_0 = \int \langle\phi|s\rangle\langle s|u\rangle\langle u|\phi'\rangle \mathrm{d}s\, \mathrm{d}u$ (the

[17] In such equation, the time is measure in units of λ^{-1}, and T is 2λ times the parameter T that we use in this paper.
[18] Even though $\phi_u(u)$ is a real function, we keep the symbol (*) in order to describe the general recipe used for the evaluation of the integral, also applicable to the integrals I_1 and I_2.

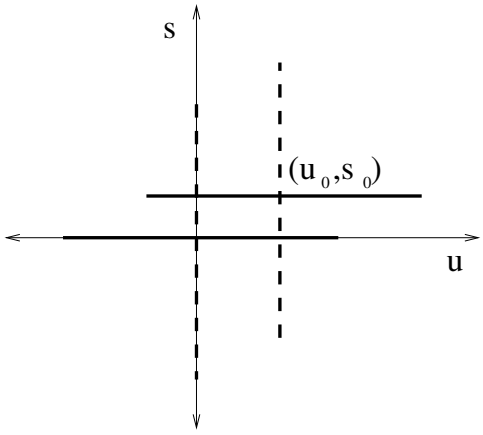

Figure 1. Crosses represent scar functions where solid lines indicate pieces of unstable manifolds and dashed lines indicate pieces of stable ones. The intersections between crosses take place at the heteroclinic points $(u_0, 0)$ and $(0, s_0)$. The area of the rectangle defined by the two crosses is the so-called heteroclinic area in [11].

s-representation of the scar state, $\langle s|\phi\rangle = \phi_s(s)$, is computed in equation (C.1)). Then, the overlap takes the form

$$I_0 = \frac{\mathrm{e}^{-\mathrm{i}s_0u_0/2\hbar}}{\sqrt{2\pi\hbar}} \int_{-\infty}^{\infty} \phi_s^*(s)\phi_u(u-u_0)\,\mathrm{e}^{-\mathrm{i}(s-s_0)u/\hbar}\,\mathrm{d}s\,\mathrm{d}u, \tag{36}$$

where the point of stationary phase at $(u = 0, s = s_0)$ is clearly shown in the integrand. Moreover, taking into account that $\phi_u(u-u_0)$ and $\phi_s(s)$ are slowly varying functions in the vicinity of $u = 0$ and $s = s_0$,[19] respectively, we can use the complex conjugate of equation (D.1), to obtain the $(0, s_0)$ contribution to the overlap as an expansion in powers of $\hbar$:

$$I_0(0, s_0) = \sqrt{2\pi\hbar}\,\mathrm{e}^{-\mathrm{i}s_0u_0/2\hbar} \sum_{n\geqslant 0} \frac{(-\mathrm{i}\hbar)^n}{n!}\phi_s^{(n)*}(s_0)\phi_u^{(n)}(-u_0).$$

We emphasize that the neighbourhood of the point $(u = u_0, s = 0)$ provides a significant contribution to I_0, which is not captured by $I_0(0, s_0)$. The reason is that even though the phase is not stationary at $(u = u_0, s = 0)$ in equation (36), the integrand is ill behaved in such a region. Nevertheless, the contribution to I_0 provided by the heteroclinic point $(u_0, 0)$ can be evaluated by Fourier transforming $\phi'_u(u)$; that is, using the relation $I_0 = \int \langle\phi|u\rangle\langle u|s\rangle\langle s|\phi'\rangle\,\mathrm{d}s\,\mathrm{d}u$. In this case, however, before applying (D.1) it is necessary to separate the rapidly oscillating contribution of $\langle s|\phi'\rangle = \phi'_s(s)$ according to equation (C.2). Then, the overlap results

$$I_0 = \frac{\mathrm{e}^{\mathrm{i}s_0u_0/2\hbar}}{\sqrt{2\pi\hbar}} \int_{-\infty}^{\infty} \phi_u^*(u)\phi_s(s-s_0)\,\mathrm{e}^{\mathrm{i}s(u-u_0)/\hbar}\,\mathrm{d}s\,\mathrm{d}u,$$

and from this, the contribution $I_0(u_0, 0)$ is derived with the assistance of (D.1).

[19] We mean that these functions are practically constants when the argument changes by $\hbar$. These conditions are clearly satisfied when $|u_0|, |s_0| > \sqrt{\hbar}$, and this is the generic situation for the short PO approach.

After a few calculations one finds $I_0(u_0, 0) = I_0^*(0, s_0)$. So, the sum of these two contributions gives us[20]

$$I_0 \simeq 2\sqrt{2\pi\hbar} \sum_{n\geqslant 0} \frac{\hbar^n}{n!} \cos\left(\frac{s_0 u_0}{2\hbar} - n\frac{\pi}{2}\right) \phi_u^{(n)}(s_0)\phi_u^{(n)}(u_0). \tag{37}$$

It is worth mentioning that this equation is an asymptotic expansion, and so it does not converge for any fixed value of $\hbar$. The error of the asymptotic expansion decreases as the number of included terms increases up to a minimum error for a given number n^* of terms, but then, the inclusion of more terms makes the approximation worse. In appendix E, we provide an estimate for n^* and for the relative error of the approximation.

The semiclassical calculation of I_1 and I_2 follows the same steps. With the assistance of the Fourier transforms given by equations (C.3) and (C.4), the final expansions for these integrals result:

$$I_1 \simeq -\mathrm{i}\sqrt{2\pi\hbar} \sum_{n\geqslant 0} \frac{\hbar^n}{n!} \sin\left(\frac{s_0 u_0}{2\hbar} - n\frac{\pi}{2}\right) \left[h_u^{(n)}(s_0)\phi_u^{(n)}(u_0) + h_u^{(n)}(u_0)\phi_u^{(n)}(s_0)\right], \tag{38}$$

and

$$I_2 \simeq 2\sqrt{2\pi\hbar} \sum_{n\geqslant 0} \frac{\hbar^n}{n!} \cos\left(\frac{s_0 u_0}{2\hbar} - n\frac{\pi}{2}\right) h_u^{(n)}(s_0)h_u^{(n)}(u_0). \tag{39}$$

The method of stationary phase does not work when $q_0 = 0$ or $p_0 = 0$. So, in the case of diagonal matrix elements (for δ and γ the same PO) when $m = m'$ and $l = j = 0$ (see equation (30)) , it is necessary to evaluate directly the integrals. Nevertheless, the calculation is trivial for the first two integrals, while appendix A discusses the other:

$$I_0 = 1, \quad I_1 = 0 \quad \text{and} \quad I_2 = \sigma_E^2. \tag{40}$$

7. The simplest scar functions

In order to clarify the relations developed up to here, let us consider periodic orbits of period one. They are γ_1 with fixed point ($q_0 = q_1 = 0$, $p_0 = p_1 = 0$), and γ_2 with fixed point ($q_0 = q_1 = 1/2$, $p_0 = p_1 = 1/2$). Then, from equations (3) and (4) it results $m = n = 0$ for γ_1 with $R(0, 0, 0, 0) = 0$, while $m = n/2 = 1$ for γ_2 with $R(1/2, 1/2, 1, 2) = 3/4$. Later, BS energies and phases are given, according to (18), by $\alpha_{\gamma_1} \equiv -\tau E_{\gamma_1}/\hbar = 0$ and $\alpha_{\gamma_2} \equiv -\tau E_{\gamma_2}/\hbar = 3/4\hbar = 3\pi N/2$. Moreover, scar functions take the simple form (see equation (15)),

$$\phi_{\gamma_1}(q) = \phi(q) \qquad \text{and} \qquad \phi_{\gamma_2}(q) = \mathrm{e}^{\mathrm{i}\pi N(q-1/2)}\phi(q - 1/2);$$

of course, $h_{\gamma_1}(q) = h(q)$ and $h_{\gamma_2}(q) = \mathrm{e}^{\mathrm{i}\pi N(q-1/2)}h(q - 1/2)$. By projecting these functions on the torus (see equation (19)), one obtains that $\overline{\phi}_{\gamma_1}(k/N)$ is always a real even function, while $\overline{\phi}_{\gamma_2}(k/N)$ is real even for even N and pure imaginary odd for odd N (by including the global phase appearing in (F.2), $\overline{\phi}_{\gamma_2}(k/N)$ is always a real function).

To have some idea of the phase space structure of these scar functions, figure 2 displays the Husimi representation of $\overline{\phi}_{\gamma_2}$, for $N = 99$.[21] The left panel, corresponding to $T = T_E$ (or equivalently to $A = 1$; see equation (14)), has a structure similar to the scar function of a hyperbolic point in the plane (where homoclinic contributions do not exist). On the other hand, the right panel which corresponds to $T = 1.5T_E$ (or $A \sim 25$), clearly shows the influence of homoclinic contributions.

[20] We use the relation $\phi_u^{(n)}(-u) = (-1)^n\phi_u^{(n)}(u)$, which is valid because $\phi_u(u)$ is even.

[21] The Husimi of $\overline{\phi}_{\gamma_2}$ at (q_1, p_1) is the square modulus of its overlap with the projection on the torus of the coherent state $\exp[-(q - q_1)^2/2\hbar + \mathrm{i}p_1 q/\hbar]$.

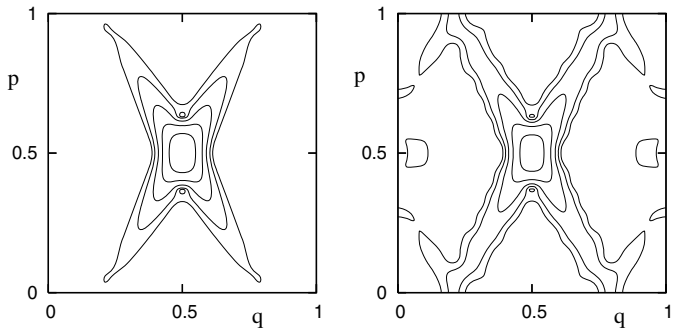

Figure 2. Contour lines in logarithmic scale of the Husimi representation of $\overline{\phi}_{\gamma_2}$, for $N = 99$. The left panel corresponds to $T = T_E$, and the right panel corresponds to $T = 1.5T_E$.

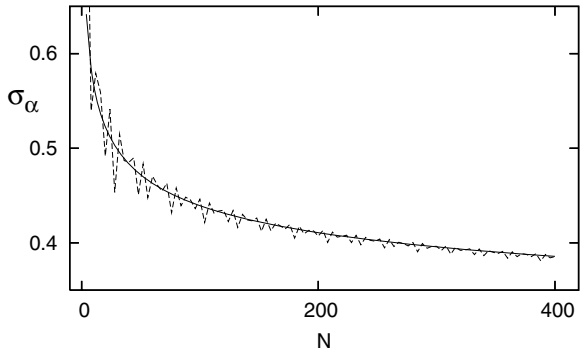

Figure 3. Phase dispersion, $\sigma_\alpha \equiv \tau\sigma_E/\hbar$, of $\overline{\phi}_{\gamma_2}$ as a function of N. The numerical computation (dashed line) according to equation (41) is compared with a prediction (solid line) given by equation (A.3). The prediction does not include homoclinic contributions.

Now, we will use these scar functions to verify semiclassical predictions; in the following, we use $T = T_E$. Figure 3 compares a numerical calculation of the phase dispersion, $\sigma_\alpha \equiv \tau\sigma_E/\hbar$, by using (22), (23) and (24):

$$\sigma_E^2(\gamma) = \frac{\langle\gamma|\hat{H}_{\rm cat}^2|\gamma\rangle}{\langle\gamma|\gamma\rangle} - \left(\frac{\langle\gamma|\hat{H}_{\rm cat}|\gamma\rangle}{\langle\gamma|\gamma\rangle}\right)^2, \tag{41}$$

with the prediction given by (A.3). As it can be seen, the prediction just describes the mean behaviour, because it only takes into account the term $l = j = 0$ of diagonal matrix elements according to (40), but the inclusion of more terms (the homoclinic contributions) certainly improves the result.

In order to verify the accuracy of the semiclassical expressions as a function of the number of included terms, let us consider the overlap $\langle\gamma_1|\gamma_2\rangle$. For this couple of POs, $q_0 = 1/2 + l$ and $p_0 = 1/2 + j$, and equation (28) reduces to

$$\langle\gamma_1|\gamma_2\rangle = \sum_{j,l} \mathrm{e}^{\mathrm{i}\pi N[j-(1/2+j)(1/2+l)]} I_0^{(l,j)}, \tag{42}$$

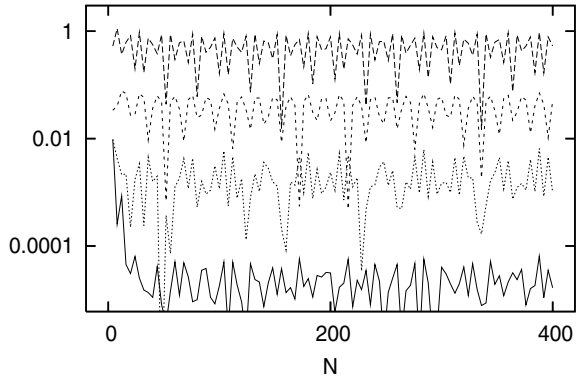

Figure 4. Error in the semiclassical evaluation of the overlap according to equation (44), as the number of heteroclinic contributions increases. The curves from top to bottom correspond to $B = 0$, $B = I_0^{(0,0)}$, $B = I_0^{(0,0)} + I_0^{(0,1)}$ and $B = I_0^{(0,0)} + I_0^{(0,1)} + I_0^{(1,0)} + I_0^{(1,1)} + I_0^{(0,2)} + I_0^{(1,2)}$, respectively.

where the dependence of I_0 on (l, j) is explicitly shown; each term of the sum consists of two heteroclinic contributions like those in figure 1. Moreover, it is easy to verify for nonnegative integers (l, j) the following relations[22]:

$$u_0^{(l,j)} = s_0^{(-l-1,j)} = -s_0^{(l,-j-1)} = -u_0^{(-l-1,-j-1)},$$

and

$$s_0^{(l,j)} = u_0^{(-l-1,j)} = -u_0^{(l,-j-1)} = -s_0^{(-l-1,-j-1)}.$$

Applying these relations to equation (37), and using the fact that the derivatives $\phi_u^{(n)}$ have defined parity, one finds

$$I_0^{(l,j)} = I_0^{(-l-1,j)} = I_0^{(l,-j-1)} = I_0^{(-l-1,-j-1)}.$$

So, we can rearrange the terms of the sum providing the overlap into groups of four terms (with the same value of I_0) labelled by the nonnegative integers (l, j). Moreover, it is easy to verify that the sum of the four coefficients in (42), $e^{i\pi N[j-(1/2+j)(1/2+l)]}$, for each group is equal to $4(-1)^{N/4}$ for N a multiple of 4, and zero otherwise. Then, the overlap results

$$\langle\gamma_1|\gamma_2\rangle = 4(-1)^{N/4} \sum_{j,l\geqslant 0} I_0^{(l,j)}, \tag{43}$$

for N a multiple of 4, and zero otherwise.

In what follows we compare the numerical computation of the overlap given by (22) with the previous equation, where the terms $I_0^{(l,j)}$ are evaluated using (37). Figure 4 displays the expression,

$$N \times \mathrm{abs}[\langle\gamma_1|\gamma_2\rangle - 4(-1)^{N/4}B], \tag{44}$$

for N a multiple of 4, where B is given by 0, $I_0^{(0,0)}$, $I_0^{(0,0)} + I_0^{(0,1)}$ and $I_0^{(0,0)} + I_0^{(0,1)} + I_0^{(1,0)} + I_0^{(1,1)} + I_0^{(0,2)} + I_0^{(1,2)}$, for the curves from top to bottom, respectively. The top curve shows that the overlap is bounded by $1/N$ in the considered range. The second curve demonstrate that the term $4(-1)^{N/4}I_0^{(0,0)}$ provides 90% of the overlap, and equivalently, the third curve

[22] From equations (31) and (30) it results $u_0^{(l,j)} = [1+2j+\alpha^2(1+2l)]/(\alpha 2^{3/2})$ and $s_0^{(l,j)} = [1+2j-\alpha^2(1+2l)]/(\alpha 2^{3/2})$, where the dependence of u_0 and s_0 on (l, j) is explicitly shown.

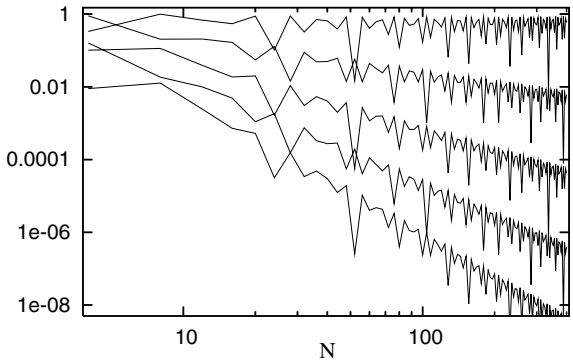

Figure 5. $4N$ times the absolute value of each term of equation (37) used for the evaluation of $I_0^{(0,0)}$; upper curve corresponds to $n = 0$ and bottom curve to $n = 4$. Each curve is bounded from above by the relation $0.9(3.5/N)^n$.

shows that $4(-1)^{N/4}\left(I_0^{(0,0)} + I_0^{(0,1)}\right)$ represents 99% of the overlap. The bottom curve indicates that the first six terms of (43) describe 99.99% of the overlap; however, for small values of N (specifically for $N = 4$, 8 and 12) we note some problems related to the asymptotic nature of equation (37). As discussed in section 6, the asymptotic expansion does not converge for any fixed value of N. In particular, for $N = 4$, the minimum error is obtain for $n^* = 4$ (this value is well predicted by (E.1)). Furthermore, this minimum error takes a relative value of around 1%, which is well predicted by (E.2).

Now, let us analyse the term $I_0^{(0,0)}$, which provides the main contribution to the overlap. Figure 5 plots $4N$ times the absolute value of each of the first five terms of (37); the upper curve corresponds to $n = 0$ and bottom curve to $n = 4$. Each curve is bounded from above by the relation $0.9(3.5/N)^n$, where the factor $3.5/N$ is understood according to [11], in terms of the heteroclinic area defined in figure 1 as follows:

$$\frac{3.5}{N} \sim 4\sqrt{3}\pi\hbar = \frac{\pi\hbar}{\left|u_0^{(0,0)} s_0^{(0,0)}\right|}.$$

This means that the asymptotic expansion guarantees an estimate of the overlap when the following relation is satisfied:

$$\pi\hbar \lesssim \text{abs(heteroclinic area)}. \tag{45}$$

The semiclassical evaluation of the other matrix elements (see equations (23) and (24)) presents exactly the same characteristics as in the case of the overlap. So, we conclude that there are two types of errors in the semiclassical evaluation of matrix elements. One is given by the truncation in the number of terms included in equation (28); that is, the number of homoclinic (for diagonal elements) or heteroclinic (for nondiagonal elements) contributions included in the calculation. As it is suggested in figure 4, this error decays exponentially with the number of included terms. The other error is related to the fact that the method of stationary phase only works when the heteroclinic point, according to equation (45), is not simultaneously close to the two POs. We notice that homoclinic areas of the order of $\hbar$ can only be found in long POs (of the order of the Heisenberg time), so the second error does not occur in the short PO approach for diagonal matrix elements.

8. The structure of eigenfunctions in terms of scar functions for $N = 25$

The objectives of this section are to show, in a simple case, the power of the short PO approach to describe the structure of eigenfunctions, and the high accuracy obtained with the Hamiltonian formulation developed in section 5.

We consider the case $N = 25$, and in order to uniformly cover the phase space let us employ a set of 25 points at rational positions $(q = i/5, p = j/5)$, with $0 \leqslant i, j < 5$. This set contains eight primitive periodic orbits of period 3, and the PO γ_1 discussed in section 7. We label with $\delta_1, \delta_2, \delta_3$ and δ_4 the POs starting at $(1/5, 0)$, $(2/5, 0)$, $(0, 1/5)$ and $(0, 2/5)$, respectively. Moreover, following the notation of section 4, $\delta_1^*, \delta_2^*, \delta_3^*$ and δ_4^* are the POs connected to the previous ones by spatial symmetry.

A straightforward calculation, following the recipe of section 4, shows that the eight POs of period 3 have the same set of BS phases given by $-2\pi/3, 0$ and $2\pi/3$; in this section we use the interval $(-\pi, \pi]$ to describe eigenphases. We can then evaluate, for instance, the corresponding scar functions for the BS phase $\alpha = 0$. Using equation (15), it results that

$$\phi_{\delta_1}(q) = \tfrac{1}{\sqrt{3}}[\phi(q - 1/5) + 2\cos(5\pi q)\, \mathrm{e}^{\mathrm{i}25q\pi}\phi(q - 2/5)],$$

$$\phi_{\delta_2}(q) = \tfrac{1}{\sqrt{3}}[\phi(q - 2/5) + 2\cos(15\pi q)\, \mathrm{e}^{\mathrm{i}25q\pi}\phi(q - 4/5)],$$

$$\phi_{\delta_3}(q) = \tfrac{1}{\sqrt{3}}\{\mathrm{e}^{\mathrm{i}10q\pi}\phi(q) + \mathrm{e}^{\mathrm{i}20q\pi}[\phi(q - 1/5) + \phi(q - 4/5)]\},$$

$$\phi_{\delta_4}(q) = \tfrac{1}{\sqrt{3}}\{\mathrm{e}^{\mathrm{i}20q\pi}\phi(q) + \mathrm{e}^{\mathrm{i}40q\pi}[\phi(q - 2/5) + \phi(q - 3/5)]\},$$

and by applying equation (19) they are projected on the torus. Moreover, the following relations can directly be verified (see equations (F.5) and (F.9)):

$$\overline{\phi}_{\delta_j}(k/N) = \overline{\phi}_{\delta_j^*}(1 - k/N) \qquad \text{for} \quad j = 1, 2 \quad \text{and} \quad k = 0, \ldots, N - 1,$$

with these functions being real functions (because the corresponding POs satisfy $\delta = \delta'$), and

$$\overline{\phi}_{\delta_j}(k/N) = \overline{\phi}^*_{\delta_j^*}(k/N) \qquad \text{for} \quad j = 3, 4 \quad \text{and} \quad k = 0, \ldots, N - 1,$$

with the real part of these functions being even and the imaginary part odd (because the corresponding POs satisfy $\delta = \delta^{*\prime}$).

Then, for $\alpha = 0$ we obtain four real scar functions with even (+) or odd (−) symmetry as follows:

$$\overline{\phi}^{(\pm)}_{\delta_j}(k/N) = \frac{\eta}{\sqrt{2}}[\overline{\phi}_{\delta_j}(k/N) \pm \overline{\phi}_{\delta_j^*}(k/N)] \qquad \text{for} \quad j = 1, 2, 3, 4, \tag{46}$$

with $\eta = -\mathrm{i}$ for (−) and $j = 3, 4$, and $\eta = 1$ otherwise.

In this way, we have a basis of 25 real scar functions with defined symmetry. There are twelve odd scar functions divided into three groups, each group associated with one of the three BS phases ($-2\pi/3, 0$ and $2\pi/3$); these groups have four functions each one (the odd functions of equation (46) being one of the groups). Moreover, there are three groups of even functions, each one also associated to one of the three BS phases; in this case, however, the group with $\alpha = 0$ contains five functions, the four given by (46) plus the scar function $\overline{\phi}_{\gamma_1}(k/N)$ of section 7.

Now, these functions being localized in the eigenphase spectrum, we can consider each of the groups mentioned before separately; note that the phase dispersion of each scar function is ~ 0.5 (for $T = T_E$) according to the estimate (A.3), while the difference between BS phases is $2\pi/3 \sim 2.1$. In other words, our basis decomposes the Hamiltonian matrix into three blocks for each symmetry class; even though this decomposition is not exact as it is for different

Table 1. Numerical comparison between four exact odd eigenvectors of the propagator for $N = 25$, and the eigenvectors obtained from diagonalizing a 4×4 Hamiltonian matrix. Second column shows for $T = T_E \sim 2\tau$ the percentage eigenphase error in units of the mean level spacing. Third column displays the square modulus of the overlap between the exact eigenvector and the Hamiltonian one. Fourth column provides the dispersion of the Hamiltonian eigenvector in units of the mean level spacing. The last three columns correspond to $T = 2T_E \sim 4\tau$.

Eigenphase	$Er\%$	$\lvert Ov\rvert^2$	σ	$Er\%$	$\lvert Ov\rvert^2$	σ
−0.366 52	0.4	0.9998	0.064	0.02	0.999 96	0.018
0.052 36	1.2	0.998	0.19	0.13	0.999 97	0.012
0.471 24	10	0.976	0.61	0.55	0.9983	0.16
0.890 12	57	0.86	1.41	0.53	0.9993	0.15

symmetry classes, the accuracy of the calculation is remarkable. As a representative example, let us consider a set of four odd scar functions with $\alpha = 0$ given in equation (46). In this case, phases are measured in the interval $(-\pi, \pi]$, although the interval $(\alpha - \pi, \alpha + \pi]$ should be considered for arbitrary α in order to move away the point of discontinuity; remember that in a Hamiltonian formulation the spectrum is not periodic. Then, matrix elements are evaluated with equations (22), (23) and (24), or just the corresponding semiclassical expressions.

By solving a 4×4 generalized eigenvalue problem for the Hamiltonian matrix $\mathcal{H}$ (because the basis is not orthogonal),

$$\mathcal{H}\psi = E\mathcal{O}\psi,$$

with $\mathcal{O}$ the overlap matrix, odd eigenvectors very close to four eigenvectors of the propagator are obtained; see table 1. Moreover, the evaluation of the dispersion of ψ (see equation (41)) gives us an estimate of the error in the calculation. In this respect, we would like to present the following heuristic expressions, which are very satisfactory in order to estimate the error:

$$1 - |Ov|^2 \sim \frac{\sigma^2}{16} \qquad \text{and} \qquad Er \lesssim \frac{\sigma^{3/2}}{4},$$

where Ov is the overlap between ψ and the exact eigenvector, and Er is the absolute value of the eigenvalue difference; the quantities Er and σ are measured in units of the mean level spacing. Note that the previous relations provide an estimate of the error in the calculation without requiring a comparison with the exact computation.

Finally, we emphasize that the diagonalization of the other blocks provides exactly the same level of accuracy.

9. Final remarks and conclusions

We have successfully applied the short periodic orbit approach for the quantum cat maps. In particular, within a Hamiltonian formulation a new perspective was presented for the semiclassical evaluation of eigenfunctions and eigenphases.

Being manifold directions fixed for the cat maps, scar functions are simply constructed with $\phi(q)$ (see equation (11)). Moreover, asymptotic expansions for the evaluation of matrix elements are given in terms of $\phi_u(u)$ (see equation (32)), the u-representation of $\phi(q)$. With respect to equation (20), where quantum dynamics is introduced by the action of the Hamiltonian on scar functions, we emphasize that it is the general recipe used by the short periodic orbit approach.

Section 7 demonstrates that matrix elements between fixed points are semiclassically given by a finite number of heteroclinic contributions. So, for POs with periods of the order

of $\ln N$, the number of heteroclinic contributions (or homoclinic contributions in the case of diagonal matrix elements) is of the order of $\ln^2 N$.

The spirit of the short periodic orbit approach is to find the best semiclassical basis, and to provide asymptotic expressions for the corresponding matrix elements. Section 8 presents an example showing the advantages of employing a basis of scar functions in place of the position basis, while [14] analyses such advantages in the semiclassical limit. Of course, it should be clear that by increasing T, the number of required scar functions decreases and eventually for T of the order of the Heisenberg time, each scar function should be an eigenfunction; however, the approach would be as cumbersome as Gutzwiller's theory. In contrast, the philosophy behind the short PO approach is to use the semiclassical dynamics whenever it is reasonable to do so, namely, up to times of the order of the Ehrenfest time, and afterward to work from a quantum point of view.

Appendix A

In this appendix, we derive an interpolation formula for the phase dispersion, $\sigma_\alpha(T)$, between the behaviour for $T \sim 0$ and $T \to \infty$, where

$$\sigma_\alpha(T) \equiv \frac{\tau\sigma_E(T)}{\hbar} = \tau\lambda\frac{\sigma_E(T)}{\lambda\hbar},$$

with $\tau\lambda = \ln(2+\sqrt{3})$ according to section 2.

We have derived in [11] the asymptotic behaviour of the energy dispersion as follows:

$$\frac{\sigma_E(T)}{\lambda\hbar} = \frac{\pi/2}{x+z} + \mathrm{O}(x^{-3}), \tag{A.1}$$

with $x \equiv \lambda T$, and

$$z = \left(\int_0^\infty \frac{y\,\mathrm{d}y}{\sqrt{\cosh(y)}}\right) \div \left(\int_0^\infty \frac{2\,\mathrm{d}y}{\sqrt{\cosh(y)}}\right) \simeq 1.060\,78.$$

On the other hand, it is not difficult to show that the Taylor expansion of $\sigma_E(T)$ around $T = 0$ is even. So, according to equation (10) it results[23]

$$\frac{\sigma_E(T)}{\lambda\hbar} = \frac{1+\mathrm{O}(x^2)}{\sqrt{2}}. \tag{A.2}$$

Then, we propose as a first step the interpolation formula,

$$f(x) = \frac{\pi/2}{x+z+\alpha/(1+x/\alpha)},$$

with $\alpha = \pi/\sqrt{2} - z \simeq 1.160\,66$, which satisfies equations (A.1) and (A.2) simultaneously.

A numerical calculation shows that the relative error of $f(x)$ is smaller than 2.5%, while it takes its greatest value in the intermediate range as expected. Finally, the heuristic expression,

$$\frac{\sigma_E(T)}{\lambda\hbar} \simeq f(x) \div [1 + 0.0268\,\mathrm{e}^{-(\ln x - 1)^2}], \tag{A.3}$$

has a relative error smaller than 0.1% for $x > 1$, and smaller than 0.4% for $x < 1$.

[23] In fact, a straightforward but tedious calculation shows that $\sigma_E(T)/(\lambda\hbar) = [1 - (3/2 - 12/\pi^2)x^2 + \mathrm{O}(x^4)]/\sqrt{2}$.

Appendix B

Let $\psi(q)$ and $\phi(q)$ be wavefunctions defined on the real line, with $\overline{\psi}(k/N)$ and $\overline{\phi}(k/N)$ the corresponding projections on the torus as described in equation (19). We will show the following relation:

$$\frac{1}{N}\sum_{k=0}^{N-1}\overline{\psi}^{*}(k/N)\overline{\phi}(k/N)=\int_{-\infty}^{\infty}\psi^{*}(q)\hat{P}\phi(q)\,\mathrm{d}q, \tag{B.1}$$

with

$$\hat{P}\phi(q)=\sum_{j,l=-\infty}^{\infty}\mathrm{e}^{\mathrm{i}2\pi Njq}\phi(q-l). \tag{B.2}$$

Note that $\mathrm{e}^{\mathrm{i}2\pi Njq}\phi(q-l)$ is a translation of $\phi(q)$, by l along the q direction and by j along the p one. So, equation (B.1) means that the overlap on the torus can be evaluated over the plane if one of the wavefunctions is replaced by the sum of all its integer translations.

By using equation (B.2) and expressing $\int_{-\infty}^{\infty}=\sum_{n=-\infty}^{\infty}\int_{n}^{n+1}$, one obtains

$$\int_{-\infty}^{\infty}\psi^{*}(q)\hat{P}\phi(q)\,\mathrm{d}q=\sum_{n=-\infty}^{\infty}\int_{n}^{n+1}\psi^{*}(q)\left[\sum_{j=-\infty}^{\infty}\mathrm{e}^{\mathrm{i}2\pi Njq}\sum_{l=-\infty}^{\infty}\phi(q-l)\right]\mathrm{d}q.$$

Then, by the change of variables $q'=q+n$ and noting that $\sum_{l=-\infty}^{\infty}\phi(q-l)$ is periodic with period unity, we have

$$\int_{-\infty}^{\infty}\psi^{*}(q)\hat{P}\phi(q)\,\mathrm{d}q=\int_{0}^{1}\left[\sum_{n=-\infty}^{\infty}\psi^{*}(q'-n)\right]\left[\sum_{j=-\infty}^{\infty}\mathrm{e}^{\mathrm{i}2\pi Njq'}\right]\left[\sum_{l=-\infty}^{\infty}\phi(q'-l)\right]\mathrm{d}q'.$$

Finally, the application of the Poisson summation formula,

$$\sum_{j=-\infty}^{\infty}\mathrm{e}^{\mathrm{i}2\pi Njq'}=\frac{1}{N}\sum_{j=-\infty}^{\infty}\delta(q'-j/N),$$

inmediately provides (B.1).

Appendix C

In this appendix, the Fourier transform of some relevant wavefunctions are evaluated. Starting with $\phi_u(u)$ (equation (32)), we have

$$\begin{aligned}\phi_s(s)&\equiv\frac{1}{\sqrt{2\pi\hbar}}\int_{-\infty}^{\infty}\phi_u(u)\,\mathrm{e}^{-\mathrm{i}su/\hbar}\,\mathrm{d}u\\&=\frac{K}{\sqrt{2}}\int_{-T}^{T}\cos\left(\frac{\pi t}{2T}\right)\left\{\frac{\mathrm{e}^{-\lambda t/2}}{(\pi\hbar)^{3/4}}\int_{-\infty}^{\infty}\exp\left[-\frac{u^2\,\mathrm{e}^{-2\lambda t}}{2\hbar}-\frac{\mathrm{i}su}{\hbar}\right]\mathrm{d}u\right\}\mathrm{d}t\\&=K\int_{-T}^{T}\cos\left(\frac{\pi t}{2T}\right)\frac{1}{(\pi\hbar)^{1/4}}\exp\left[-\frac{s^2\,\mathrm{e}^{2\lambda t}}{2\hbar}+\frac{\lambda t}{2}\right]\mathrm{d}t\\&=\phi_u(s),\end{aligned} \tag{C.1}$$

where the last step is reached after the change of variable, $t\to -t$. On the other hand, with the rename $u-u_0\to u$, the Fourier transform of $\phi'_u(u)$ (see equation (35)) inmediately results

$$\phi'_s(s)=\mathrm{e}^{-\mathrm{i}(s-s_0/2)u_0/\hbar}\phi_s(s-s_0). \tag{C.2}$$

The Fourier transform of $h_u(u)$ (see equation (33)) is simply derived by applying $i\lambda\hbar(1/2 + s\,d/ds)$ (the s-representation of $\hat{H}$) to $\phi_s(s)$. It results

$$h_s(s) = -h_u(s). \tag{C.3}$$

And finally, the Fourier transform of $h'_u(u) = e^{is_0(u-u_0/2)}h_u(u-u_0)$ is

$$h'_s(s) = e^{-i(s-s_0/2)u_0/\hbar}h_s(s-s_0). \tag{C.4}$$

Appendix D

In this appendix, we prove the following $\hbar$ expansion:

$$\int f(u)g(s)\,e^{isu/\hbar}\,ds\,du = 2\pi\hbar\sum_{n\geqslant 0}\frac{(i\hbar)^n}{n!}f^{(n)}(0)g^{(n)}(0), \tag{D.1}$$

where f and g are smooth functions.

By writing f and g in terms of Taylor expansions around zero, the integral results

$$\int f(u)g(s)\,e^{isu/\hbar}\,ds\,du = \sum_{n,m\geqslant 0}\frac{1}{n!m!}f^{(n)}(0)g^{(m)}(0)\int u^n s^m e^{isu/\hbar}\,ds\,du.$$

So, to prove (D.1) we need to prove

$$\int u^n s^m\,e^{isu/\hbar}\,ds\,du = 2\pi\hbar(i\hbar)^n n!\delta_{n,m}. \tag{D.2}$$

We differentiate n times the identity,

$$\int e^{isu/\hbar}\,du = 2\pi\hbar\delta(s),$$

to obtain

$$\int u^n\,e^{isu/\hbar}\,du = 2\pi\hbar(-i\hbar)^n\delta^{(n)}(s).$$

Then, multiplying the last equation by s^m and taking the integral with respect to s, one finds

$$\int u^n s^m e^{isu/\hbar}\,ds\,du = 2\pi\hbar(-i\hbar)^n\int s^m\delta^{(n)}(s)\,ds.$$

Finally, using the identity $\int s^m\delta^{(n)}(s)\,ds = (-1)^n n!\delta_{n,m}$ (obtained by integration by parts), equation (D.2) is proved.

Appendix E

In this appendix, let us estimate the optimal number of terms, n^*, included in the asymptotic expansion (37) in order to minimize the error; moreover, we will provide an estimate of the relative error. We guess that the obtained expressions can also be employed for the asymptotic expansions given in equations (38) and (39).

Let us to approximate the scar function by $\phi_u(u) = 1/\sqrt{|u|}$. In such a case, the integral of equation (34) takes the value [11]

$$I_0 = \pi(J_0(\alpha) - Y_0(\alpha)),$$

with $\alpha = |u_0 s_0|/2\hbar$, and where $u_0 s_0$ is the heteroclinic area appearing in figure 1; J_0 and Y_0 are the Bessel and Neumann functions of zero order, respectively. On the other hand, the asymptotic expansion of equation (37) takes the explicit form

$$I_0 \simeq 2\sqrt{\pi/\alpha} \sum_{n \geqslant 0} B(n) \cos(\alpha - n\pi/2),$$

with

$$B(n) = \frac{[(2n-1)!!]^2}{n! 2^{3n} \alpha^n};$$

that is, $B(0) = 1$, $B(1) = 1/8\alpha$, $B(2) = 9/128\alpha^2$, and so on.

A numerical computation shows us that the error of the expansion has the following sharp upper bound:

$$\text{error}(n_1) = \left| I_0 - 2\sqrt{\pi/\alpha} \sum_{n=0}^{n_1} B(n) \cos(\alpha - n\pi/2) \right| \leqslant 2\sqrt{\pi/\alpha} B(n_1 + 1).$$

Then, the minimum error is obtained for $B(n^* + 1)$ being a minimum; that is, for

$$n^* \sim 2\alpha = |u_0 s_0|/\hbar. \tag{E.1}$$

Finally, as the amplitude of I_0 is well reproduced by $2\sqrt{\pi/\alpha}$ (without including the oscillatory factor), the relative error results

$$\text{relative error}(n_1) \lesssim B(n_1 + 1). \tag{E.2}$$

Appendix F

In this appendix, we provide some recipes in order to obtain real scar functions within a defined symmetry class. We use the notation of section 4, and by convention $\gamma = \gamma'$ means that they are the same PO up to a shift of the initial point.

F.1. The $\gamma = \gamma'$ case

Let us consider a PO γ which is invariant by time reversal. The corresponding scar function, given by equations (15) and (19), is real up to a global phase; our objective is to obtain such a phase. Specifically, we have to find the real number φ such that

$$\sqrt{n}\, \mathrm{e}^{\mathrm{i}\varphi} \overline{\phi}_\gamma(k/N) = \sum_{l=-\infty}^{\infty} \sum_{j=0}^{n-1} \mathrm{e}^{\mathrm{i}\varphi + \mathrm{i}2\pi N[S_j + p_j(k/N - q_j - l)]} \phi(k/N - q_j - l) \tag{F.1}$$

is real.

The cancellation of the imaginary part in (F.1) is not the consequence of a collective contribution of many terms. In contrast, each term characterized by $(q_j + l, p_j)$ plus the corresponding time reversal term $(q_j + l, (1 - p_j)_{(\mathrm{mod}\,1)})$ [24] should be real if an appropriate global phase is selected. So, let us consider the term (q_0, p_0), where $S_0 = 0$ (see section 4). For $p_0 = 0$ or $p_0 = 1/2$, there is only one term given by

$$\exp[\mathrm{i}\varphi + \mathrm{i}2\pi N p_0(k/N - q_0)] \phi(k/N - q_0), \tag{F.2}$$

[24] We keep the operation (mod 1) on the p variable, because each term of (F.1) is periodic in p.

and it is real for $\varphi = 0$ (when $p_0 = 0$) or $\varphi = \pi N q_0$ (when $p_0 = 1/2$). On the other hand, for $p_0 \neq 0$ and $p_0 \neq 1/2$, the sum of the terms characterized by (q_0, p_0) and $(q_0, 1 - p_0)$ results

$$2\exp[\mathrm{i}\varphi + \mathrm{i}\pi N(S + k/N - q_0)]\phi(k/N - q_0)\cos[2\pi N(p_0 - 1/2)(k/N - q_0) - \pi N S], \tag{F.3}$$

and it is real for $\varphi = \pi N(q_0 - S)$, with S the reduced action for going from (q_0, p_0) to $(q_0, 1 - p_0)$.

F.2. The $\gamma = \gamma' \neq \gamma^*$ case

By including global phases, real scar functions of γ and γ^* are given (γ^* is also time reversal); see appendix F.1. Then, linear combinations of these scar functions provide real functions within defined symmetry classes. Our objective is to find those linear combinations.

In order to obtain a relation between the scar functions, let us compare the term (q_0, p_0) (plus its time reversal one) of $\overline{\phi}_\gamma$, with the corresponding term by spatial symmetry, $(q_0^*, p_0^*) = (1 - q_0, 1 - p_0)$ (mod 1), of $\overline{\phi}_{\gamma^*}$. For $p_0 = 1/2$ it results $p_0^* = 1/2$, so these terms are given from (F.2) by

$$\mathrm{e}^{\mathrm{i}\pi N(k/N)}\phi(k/N - q_0), \qquad \text{for} \quad \overline{\phi}_\gamma(k/N),$$

and

$$\mathrm{e}^{\mathrm{i}\pi N(k/N)}\phi(k/N - 1 + q_0) = (-1)^N\,\mathrm{e}^{\mathrm{i}\pi N(1-k/N)}\phi(1 - k/N - q_0), \qquad \text{for} \quad \overline{\phi}_{\gamma^*}(k/N),$$

where the even parity of ϕ was used. So, the following relation is derived for $p_0 = 1/2$:

$$\overline{\phi}_{\gamma^*}(k/N) = (-1)^N\overline{\phi}_\gamma(1 - k/N). \tag{F.4}$$

Working in the same way for $p_0 = 0$, we obtain

$$\overline{\phi}_{\gamma^*}(k/N) = \overline{\phi}_\gamma(1 - k/N). \tag{F.5}$$

Moreover, using equation (F.3) for the $p_0 \neq 0$ and $p_0 \neq 1/2$ cases, relation (F.4) is derived again.

Finally, from equations (F.4) and (F.5), even (+) real scar functions and odd (−) ones are given by

$$\overline{\phi}_\gamma^{(\pm)}(k/N) = \tfrac{1}{\sqrt{2}}[\overline{\phi}_\gamma(k/N) \pm (-1)^N\overline{\phi}_{\gamma^*}(k/N)], \qquad \text{for} \quad p_0 \neq 0, \tag{F.6}$$

and

$$\overline{\phi}_\gamma^{(\pm)}(k/N) = \tfrac{1}{\sqrt{2}}[\overline{\phi}_\gamma(k/N) \pm \overline{\phi}_{\gamma^*}(k/N)], \qquad \text{for} \quad p_0 = 0. \tag{F.7}$$

F.3. The $\gamma = \gamma^{*\prime} \neq \gamma^*$ case

By including appropriate global phases, scar functions of γ and γ^* have even real part and odd imaginary part. Furthermore, linear combinations of them provide real scar functions within defined symmetry classes.

Our starting point is equation (F.1), and we look for φ such that equation (F.1) takes a real value at $q_k \equiv k/N = 0$. As in the previous subsections we reduce the analysis to couples of terms; in this case, $(q_j + l, p_j)$ and $(-q_j - l, p_j)$.[25] Then, by using the initial point of γ, (q_0, p_0), plus the corresponding term $(-q_0, p_0)$, one obtains, for $k = 0$,

$$\mathrm{e}^{\mathrm{i}\varphi}\phi(q_0), \qquad \text{for} \quad q_0 = 0$$

[25] The existence of these couples of terms is guaranteed by the symmetry of γ.

and

$$2\exp[\mathrm{i}(\varphi+\pi NS)]\phi(q_0)\cos[\pi N(2p_0q_0+S)] \quad \text{otherwise},$$

where S is the reduced action for going from (q_0, p_0) to $(1-q_0, p_0)$ (mod 1). From these relations it results

$$\varphi = -\pi NS, \tag{F.8}$$

with $S = S_0 = 0$ for $q_0 = 0$ or $q_0 = 1/2$.

Now, by comparing the scar functions of γ and γ^*, both of them with the corresponding global phase discussed before, one finds

$$\overline{\phi}_{\gamma^*}(k/N) = \mathrm{e}^{\mathrm{i}(\varphi^*-\varphi+2\pi Nq_0)}\overline{\phi}^*_{\gamma}(k/N), \tag{F.9}$$

with φ^* the global phase of γ^*.[26] The phase $\varphi^* - \varphi + 2\pi Nq_0$ is an integer multiple of π; in particular, it is equal to $2\pi Nq_0$, for $q_0 = 0$ or $q_0 = 1/2$. Then, even (+) real scar functions and odd (−) real ones are given by

$$\overline{\phi}^{(+)}_{\gamma}(k/N) = \frac{1}{\sqrt{2}}[\overline{\phi}_{\gamma}(k/N) + \mathrm{e}^{\mathrm{i}(\varphi^*-\varphi+2\pi Nq_0)}\overline{\phi}_{\gamma^*}(k/N)], \tag{F.10}$$

and

$$\overline{\phi}^{(-)}_{\gamma}(k/N) = \frac{-\mathrm{i}}{\sqrt{2}}[\overline{\phi}_{\gamma}(k/N) - \mathrm{e}^{\mathrm{i}(\varphi^*-\varphi+2\pi Nq_0)}\overline{\phi}_{\gamma^*}(k/N)]. \tag{F.11}$$

F.4. The $\gamma = \gamma' = \gamma^*$ case

Let $\overline{\phi}_{\gamma}(k/N)$ be real by the inclusion of the global phase φ proposed in appendix F.1. As a consequence of the full symmetry of the PO, this scar function is not only real, but also belongs to a defined symmetry class. The objective is to provide a criterion in order to know whether the function is even (+) or odd (−).

In this case, related to the term (q_0, p_0) there are three more connected by time reversal $(q_0, 1-p_0)$, spatial symmetry $(1-q_0, 1-p_0)$ and both symmetries $(1-q_0, p_0)$. Actually, we can identify this situation with that appearing in appendix F.2 as follows. The terms, (q_0, p_0) and $(q_0, 1-p_0)$, belong to the real scar function of γ, and the other two terms to the real scar function of γ^*. Of course, in this case we cannot select the relative phase between scar functions, because γ and γ^* are the same PO; in contrast, this phase is fixed by the dynamics. By computing such a phase, we obtain the following relation:

$$\overline{\phi}_{\gamma}(k/N) = \mathrm{e}^{\mathrm{i}2(\varphi-\varphi')}\overline{\phi}_{\gamma}(1-k/N),$$

with φ appearing in (F.2) or (F.3), and φ' given by (F.8). As the phase $2(\varphi-\varphi')$ is an integer multiple of π, the parity of $2(\varphi-\varphi')/\pi$ gives us the parity of the scar function.

F.5. Summarizing

Equations (F.6), (F.7), (F.10) and (F.11) provide real scar functions within a defined symmetry class for all BS energies (or phases), while appendix F.4 shows that the parity of the scar function depends on the BS energy for fully symmetric POs.

Neither the $\gamma = \gamma^* \neq \gamma'$ case nor the situation without symmetries was discussed because they are only required for $N \gtrsim 10^4$. In order to illustrate this fact, table F1 displays the number of POs with a defined set of symmetries, as a function of the period. Now, taking into account that the length of a PO (see section 4) is n times the number indicated in each column with the symbol (×), the shortest length of a PO in column D or E results 16.

[26] $\varphi^* = -\pi NS^*$, with S^* the reduced action for going from $(q_0^*, p_0^*) = (1-q_0, 1-p_0)$ (mod 1) to $((1-q_0)^*, p_0^*) = (q_0, 1-p_0)$ (mod 1).

Table F1. Number of primitive periodic orbits with a defined set of symmetries, as a function of the period, n. Column A corresponds to $\gamma = \gamma' = \gamma^*$, B to $\gamma = \gamma' \neq \gamma^*$, C to $\gamma = \gamma^{*\prime} \neq \gamma^*$, D to $\gamma = \gamma^* \neq \gamma'$, and column E is the case without symmetries. The symbol $(\times)$ indicates the number of POs used for the construction of real scar functions within a defined symmetry class.

n	A $(\times 1)$	B $(\times 2)$	C $(\times 2)$	D $(\times 2)$	E $(\times 4)$
1	2	0	0	0	0
2	3	2	0	0	0
3	0	8	8	0	0
4	3	18	12	0	12
5	0	36	36	0	72
6	8	82	54	0	296
7	0	140	140	0	1160
8	18	346	242	8	4068

References

[1] Gutzwiller M C 1990 *Chaos in Classical and Quantum Mechanics* (New York: Springer)
[2] Berry M V 1985 *Proc. R. Soc.* A **400** 229
[3] Bogomolny E B 1988 *Physica* D **31** 169
[4] Voros A 1988 *J. Phys. A: Math. Gen.* **21** 685
[5] Berry M V and Keating J P 1990 *J. Phys. A: Math. Gen.* **23** 4839
[6] Vergini E G and Wisniacki D A 1998 *Phys. Rev.* E **58** R5225
[7] Vergini E G 2000 *J. Phys. A: Math. Gen.* **33** 4709
[8] Vergini E G and Carlo G G 2000 *J. Phys. A: Math. Gen.* **33** 4717
[9] Vergini E G and Carlo G G 2001 *J. Phys. A: Math. Gen.* **34** 4525
[10] Rivas A M F 2007 *J. Phys. A: Math. Theor.* **40** 11057
[11] Vergini E G and Schneider D 2005 *J. Phys. A: Math. Gen.* **38** 587
[12] Hannay J H and Berry M V 1980 *Physica* D **1** 267
[13] Yakubovich V A and Starzhinskii V M 1975 *Linear Differential Equations with Periodic Coefficients* (New York: Wiley)
[14] Vergini E G 2004 *J. Phys. A: Math. Gen.* **37** 6507